PROCEEDINGS OF SCIENCE

Emission from the jets of Low-luminosity Active Galactic Nuclei

Gunjan Tomar,[a,*] **Nayantara Gupta**[a] **and Raj Prince**[b]

[a] *Astronomy and Astrophysics department, Raman Research Institute, 5th cross road, C.V. Raman Road, Bengaluru, Karnataka - 560080*

[b] *Center for Theoretical Physics, Polish Academy of Sciences, Warsaw, Poland*

E-mail: gunjan@rri.res.in

Low-Luminosity Active Galactic Nuclei (LLAGNs) are challenging to study due to their faintness despite occupying 40% of the local Universe. The radiatively inefficient accretion flows that power these LLAGNs are known to be efficient at producing bipolar jets. Multi-wavelength observations of the jets act as a crucial probe of the physical mechanism in these extreme environments. The recent detection of LLAGNs NGC 315 and NGC 4261 in gamma rays by Fermi-LAT allows us to model their multi-wavelength spectral energy distribution (SED) from radio to gamma rays. We find that the synchrotron and synchrotron self-Compton emission from an emission region at sub-parsec scale jet can explain the SEDs up to a few GeV, leaving an excess beyond that. The gamma rays produced by the upscattering of the starlight photons from the host galaxy by the ultra-relativistic electrons at the kilo-parsec scale successfully explain this excess. Thus, similar to luminous AGNs, the electrons in the kilo-parsec jets of LLAGNs are also accelerated to ultra-relativistic energies. The ejection of a discrete knot from another LLAGN, M81*, again suggests similarities in the jet production mechanism for luminous AGNs and LLAGNs. Due to non-detection in gamma rays, we model its multi-wavelength SEDs from radio to X-rays at different epochs during the knot ejection to infer the properties of the jet. We also model the SEDs during other X-ray flaring periods identified from the long-term Swift light curve. As seen in the high-synchrotron-peaked blazars (a sub-class of luminous AGNs), the synchrotron emission from relativistic electrons from a single zone explains the SEDs from radio to X-ray during all states. We present these results and compare the similarities of these jets in LLAGNs with those produced in luminous AGNs.

38th International Cosmic Ray Conference (ICRC2023)
26 July - 3 August, 2023
Nagoya, Japan

ICRC2023
38th International Cosmic Ray Conference
The Astroparticle Physics Conference

*Speaker

© Copyright owned by the author(s) under the terms of the Creative Commons Attribution-NonCommercial-NoDerivatives 4.0 International License (CC BY-NC-ND 4.0).

PoS(ICRC2023)947

1. Introduction

Low-Luminosity Active Galactic Nuclei (LLAGNs) are fainter than their luminous counterparts due to underfed supermassive black hole at their centers which are accreting material at low, sub-Eddington accretion rates. Due to low accretion rate, the accretion flows powering these sources are radiatively inefficient. These radiatively inefficient accretion flows are known to be efficient in producing bipolar jets. The observations of these jets across multiwavelength play a pivotal role in unraveling the physical mechanisms at play within these extreme environments. By scrutinizing the differnces and similarities between luminous AGNs and low-luminoisty AGN, we can enhance our understanding on the mechanisms of jet production, evolution of the AGN population among bridging other gaps between the two. The modeling of broadband SED helps to constrain the physical parameters of the jets in these system.
For this purpose, we study five LLAGNs from Palomar survey of the nearby galaxies in [3] and [4]. Out of which only four (NGC 315, NGC 4261, NGC 1275 and M87) have been detected in gamma-ray thus far. Since NGC 1275 and M87 (NGC 4487) have been identified and studied as gamma-ray emitters before, NGC 315 and NGC 4261 are identified as gamma ray emitters for the first time by [1]. Therefore, in this paper, we only discuss the SED modeling of NGC 315 and NGC 4261.

Furthermore, although M81* have not been detected in gamma rays till now, ejection of discrete radio knot from it has been observed hinting towards similarities between jet production and/or emission mechanism of this LLAGN with the luminous AGNs where jets are known to be discrete unlike continuous in LLAGNs [2]. We construct the SED of M81* at different epochs during the knot ejection and other identified X-ray flares. We model these SEDs to constrain the physical parameters of the jet during this period. This allows us to study the variation of the jet parameters during the knot ejection in LLAGN and strike a comparison with the luminous AGNs.

2. Multiwavelength Observations of the Sample

2.1 NGC 315 and NGC 4261

For both NGC 315 and NGC 4261, we analyse ~12 years of Fermi-LAT data [2008 August 4 to 2020 August 21] with fermitools v2.0.0 and fermipy v1.0.0 following the standard procedure. In order to obtain the spectral parameters and the significance of detection of the source, a binned maximum likelihood analysis is performed by taking into account all the sources included in the updated forth source catalog (4FGL-DR2) and lying up to 5° outside the region of interest (ROI).

Additionally, X-ray data taken by XMM-Newton on 2019 January 27 (Obs ID: 369082187170) for NGC 315 is also analysed. The source and background events are extracted from a circle of radius 25 arcsec centred on the source and 50 arcsec on the same CCD away from the source, respectively for all the three European Photon Imaging Cameras (EPICs - PN, MOS1 and MOS2). All the three EPIC spectra were fitted simultaneously allowing for a cross-normalisation between them. The spectra is fitted with model `(ztbabs*po)+mekal` with a reduced-χ^2 value 1.18 (190 d.o.f).

The data at other wavelengths in both the cases are compiled from the previous observations (for details see [3]).

PoS(ICRC2023)947

2.2 M81*

2.3 Gamma Ray

We analyse 13.5 years of Fermi-LAT data [2008 August 4 to 2022 February 28] with fermitools v2.0.0 and fermipy v1.0.0 following the standard procedure. Due to proximity of strong gamma ray emitter M82 and larger point spread function than the separation between the two at low energies, we only select events with energies greater than 10 GeV. Since the source does not belong to any catalog, we manually add a point source at the RA, Dec of M81*. The source is modeled with a power-law. We derive an upper limit on gamma ray flux of M81* as 2.58×10^{-13} erg cm^{-2} s^{-1}.

2.4 X-ray and UV-Optical

M81* has been monitored by X-Ray Telescope (XRT) instrument onboard Swift telescope several times between 2005 April 21 and 2021 May 24, in both photon counting and windowed timing mode. We extract the source and background events for all the available observations following the standard procedure (for details see [4]). The spectra were obtained from the corresponding event files using the XSELECT v2.4g software. All the observations are checked and corrected, if needed for pile-up effect. The spectra were fit using an absorbed power-law model in XSPEC using Cash statistics. To construct the long term lightcurve in X-ray unabsorbed power-law flux in both soft (0.2-5.0 keV) and hard (5.0 - 10.0 keV) X-ray bands are then plotted for each observations (see Figure 2).

The source was monitored by Swift-UVOT simultaneous to multiple XRT observations in some or all of the six filters. We derive the magnitudes using `uvotsource`, which are the corrected for Galactic extinction and using the reddening law wit R_v= 3.1. The magnitudes are then converted to fluxes and plotted in the multiwavelength lightcurve (Figure 2).

3. Modeling the Multi-wavelength SEDs

For the leptonic modeling of the sample, we use a publicly available time-dependent code GAMERA.

3.1 NGC 315 and NGC 4261

Through leptonic modeling, we demonstrate that the synchrotron and synchrotron self-Compton emissions originating from an emission region at the sub-parsec scale within the jet can adequately explain the observed SEDs up to a few GeV. However, an excess beyond this energy range remains unexplained.

To address the unexplained excess gamma-ray emission, we propose an inverse-Compton component involving the upscattering of starlight photons from the host galaxy by ultra-relativistic electrons located at the kilo-parsec scale within the jet. This finding implies that, similar to luminous AGNs, the electrons in the kilo-parsec jets of LLAGNs are accelerated to ultra-relativistic energies. The parameters obtained are shown in Table 1 and Table 2.

PoS(ICRC2023)947

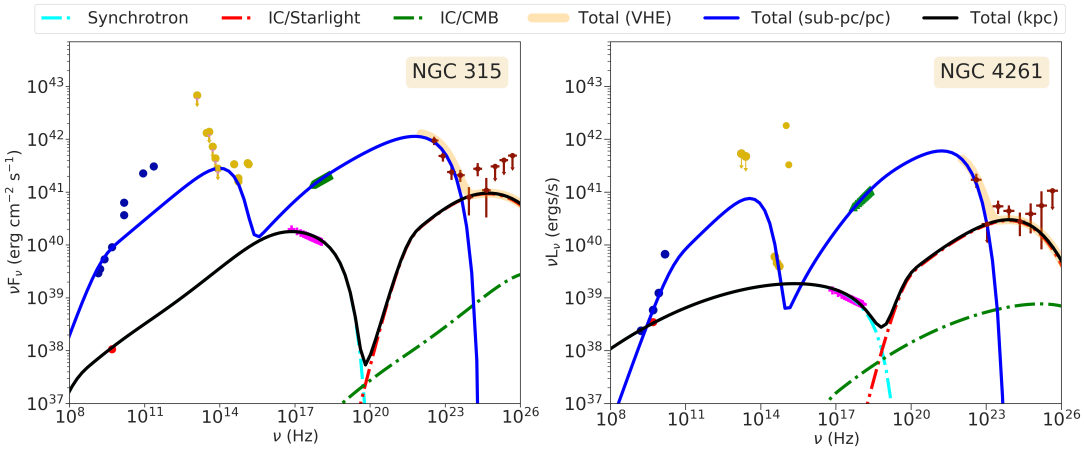

Figure 1: Leptonic model including emission from an emission region at sub-parsec scale (blue curve) and at kilo-parsec scale (black curve) from NGC 315 and NGC 4261.

3.2 M81*

The ejection of a discrete knot from another LLAGN, M81* provides further evidence for similarities in the jet production mechanisms between luminous AGNs and LLAGNs [2]. Despite the non-detection of gamma rays from M81*, we perform detailed modeling of its multi-wavelength SEDs from radio to X-rays at different epochs during the knot ejection event to infer the properties of the jet.

Additionally, we identify X-ray flaring periods in the longterm X-ray lightcurve using astropy implementation of the Bayesian Block alogorithm. Although, the X-ray flux during know ejection period is not statistically signficant, we call it Flare A to obtain the parameters of jet during the knot ejection period.

We model the SEDs for different epochs during the knot ejection and X-ray flaring periods of M81* obtained from the long-term Swift light curve. This analysis provides valuable insights into the behavior and dynamics of the jet during these active phases. The model parameters are given in Table 3.

4. Conclusions

In this proceedings paper, we have presented our findings from the multi-wavelength analysis of LLAGNs, with a specific focus on NGC 315, NGC 4261, and M81*. Our study highlights the importance of multi-wavelength observations in unraveling the physical mechanisms operating within the extreme environments of the jets in these sources. The detection of gamma rays from NGC 315 and NGC 4261, and the modeling of SEDs from radio to gamma rays, have allowed us to gain insights into the jet properties of LLAGNs. Furthermore, our analysis of M81*, during the knot ejection event and X-ray flaring periods, has provided valuable information regarding the behavior and dynamics of the jet.

Our analysis reveals that the synchrotron and synchrotron self-Compton emissions originating from an emission region at the sub-parsec scale within the jet adequately account for the SEDs up to

PoS(ICRC2023)947

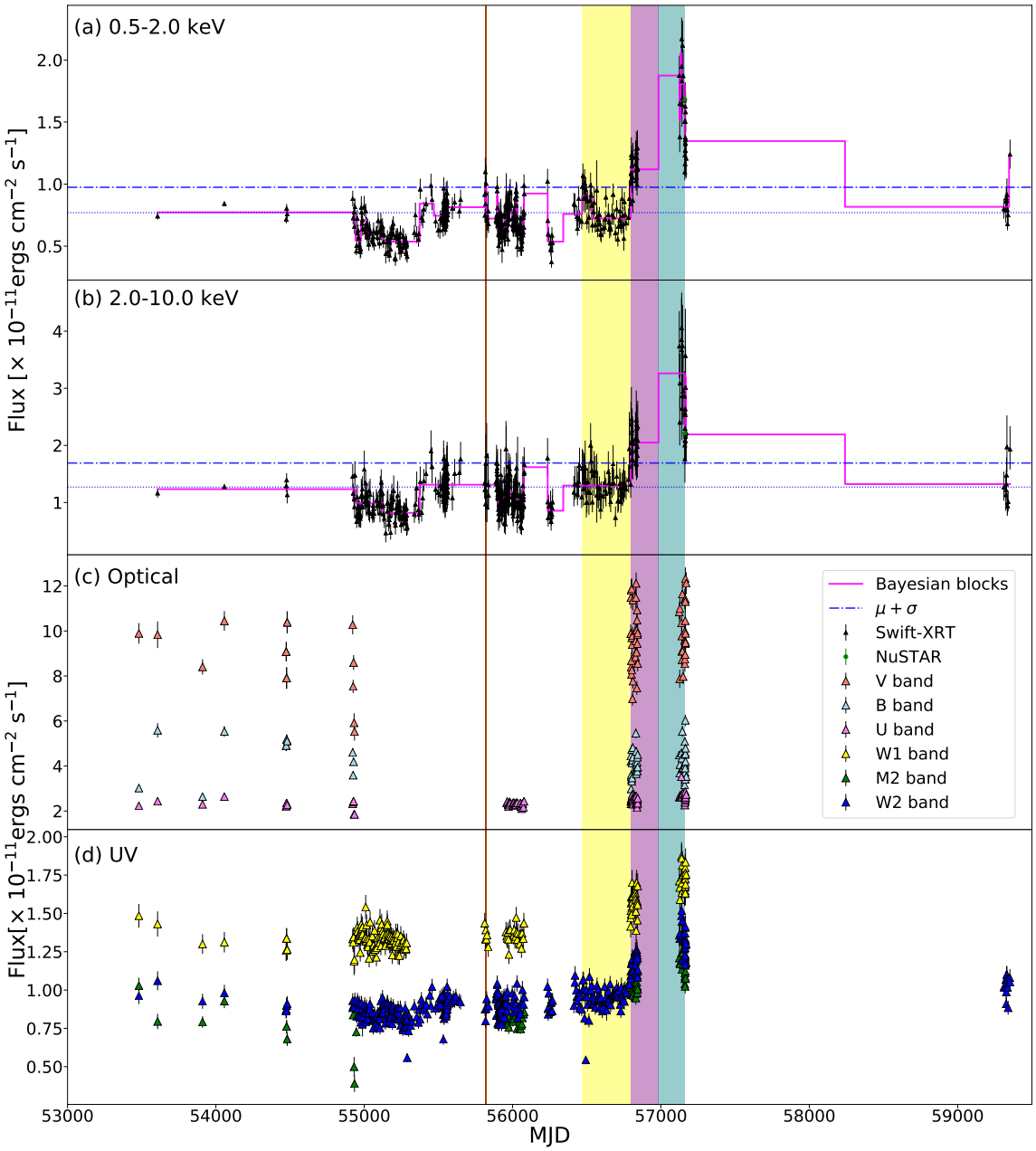

Figure 2: The lightcurve in (a) soft X-ray energies (0.5-2.0 keV) and (b) hard X-ray energies (2.0-10.0 keV). The light curve in Optical (c) and UV (d). The yellow region represents the quiescent state (MJD 56467.7 - MJD 56796.7). The brown line (MJD 55814.83 - MJD 55823.35), and the purple (MJD 56796.74 - MJD 56983.37) and teal (MJD 56983.37 - MJD 57160.25) shaded regions represent Flare A, Flare B, and Flare C, respectively.

PoS(ICRC2023)947

Parameter	NGC 315	NGC 4261
Q_i	Power-Law	Power-Law
γ_{min}	35	190
γ_{max}	2.5×10^4	1.6×10^4
η_{esc}	1	1
α	2.2	2.06
Γ_b	1.5	1.5
δ	1.6	1
R(cm)	1.1×10^{16}	1×10^{16}
B (G)	0.21	0.21
P_e(ergs/s)	3.9×10^{37}	4.8×10^{37}
P_B(ergs/s)	4.5×10^{40}	3.72×10^{40}
P_p (ergs/s)	4.7×10^{38}	1.12×10^{38}
P(ergs/s)	4.5×10^{40}	3.74×10^{40}

Table 1: Parameter values for the best-fit one-zone leptonic model for sub-parsec jet.

Parameter	NGC 315	NGC 4261
U_{star}(ergs/s)	2.25×10^{-9}	2.09×10^{-10}
γ_{min}	1400	220
γ_{max}	5.0×10^8	5.2×10^8
α	2.1	2.16
β	0.025	0.084
B (G)	10×10^{-6}	7.1×10^{-6}
R (cm)	5×10^{21}	1×10^{21}
η_{esc}	1	1
Γ_b	1.5	1.5
δ	1.6	1
$P_{tot(kpc)}$ (ergs/s)	2.1×10^{43}	4.25×10^{41}

Table 2: Parameter values for the best-fit one-zone leptonic model for kilo-parsec jet.

a few GeV. However, an unexplained excess is observed beyond this energy range. To address this excess, we propose that gamma rays are produced through the upscattering of starlight photons from the host galaxy by ultra-relativistic electrons at the kilo-parsec scale. This finding indicates that, akin to luminous AGNs, the electrons within the kilo-parsec jets of LLAGNs are also accelerated to ultra-relativistic energies.

Furthermore, we investigate the ejection of a discrete knot from another LLAGN, M81*, which suggests similarities in the jet production mechanisms between luminous AGNs and LLAGNs. Despite the non-detection of M81* in gamma rays, we perform multi-wavelength modeling of its SEDs, spanning from radio to X-rays, at different epochs during the knot ejection event to infer the properties of the jet. Additionally, we model the SEDs during other X-ray flaring periods identified from the long-term Swift light curve. Drawing parallels with observations of high-synchrotron-peaked blazars (HSPs), a sub-class of luminous AGNs, we demonstrate that the synchrotron emission from relativistic electrons within a single zone can explain the observed SEDs from radio to X-rays across all states (Figure 3). In line with observations of HSPs, we find that the M81* shows similar harder-when-brighter behavior in X-rays. The synchrotron peak frequency increases with the X-ray luminosity as is seen for the HSPs (Figure 4).

References

[1] de Menezes R., Nemmen R., Finke J. D., Almeida I., Rani B., 2020, MNRAS, 492, 4120. doi:10.1093/mnras/staa083

[2] King A. L., Miller J. M., Bietenholz M., Gültekin K., Reynolds M. T., Mioduszewski A., Rupen M., et al., 2016, NatPh, 12, 772. doi:10.1038/nphys3724

[3] Tomar G., Gupta N., Prince R., 2021, ApJ, 919, 137. doi:10.3847/1538-4357/ac1588

PoS(ICRC2023)947

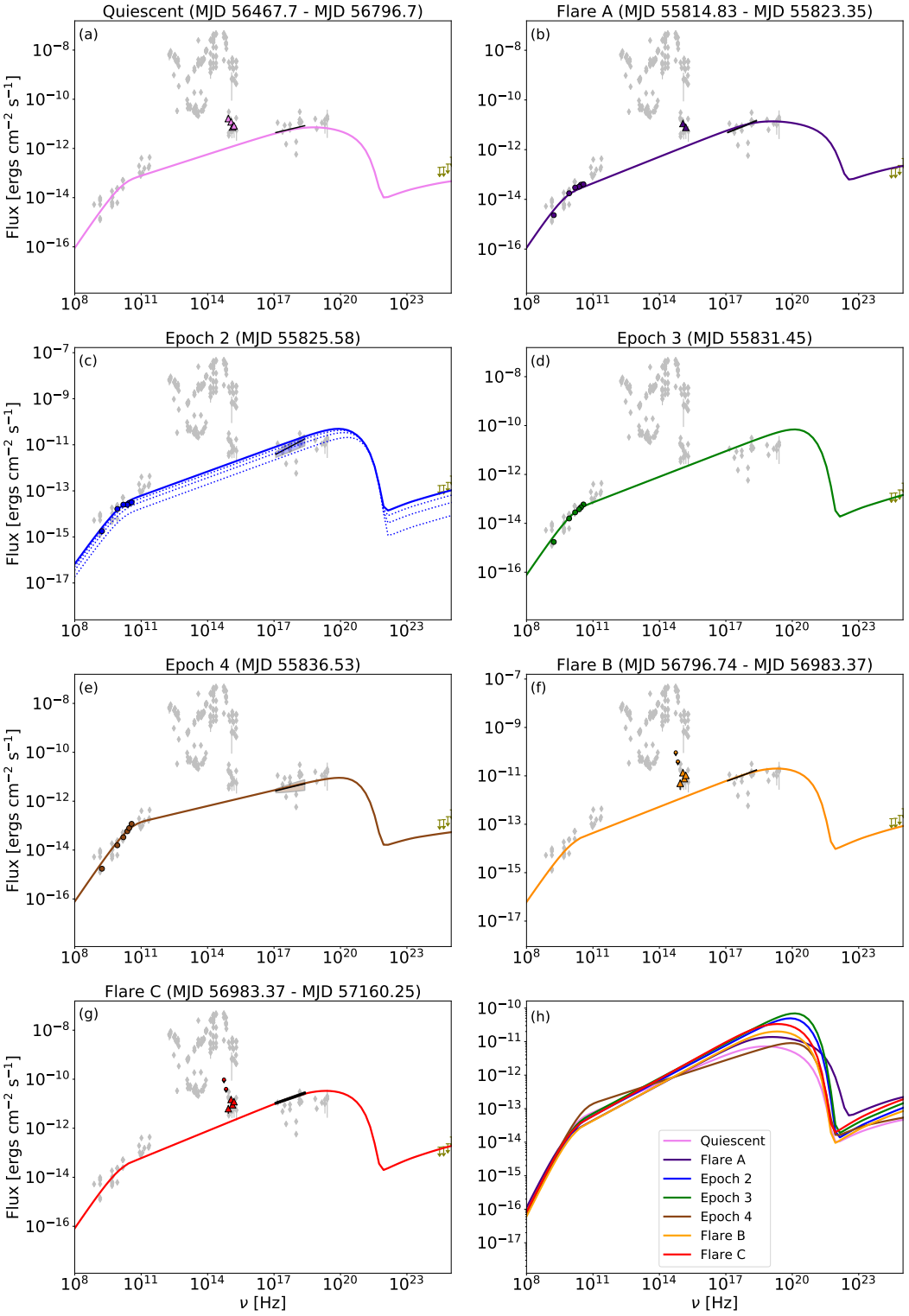

Figure 3: One zone SED modeling of M81* during different states. Panel c: The dotted curves in the modeling represent the evolution of SED from the initial time of injected electrons to the final age of the system, which explains the emission at this epoch. Panels a-g: X-ray data for different states are shown in black. The upper limits obtained using Fermi-LAT data are shown in olive to constrain the SSC component and thus, the size of the emission region. Panel h: Simulated SEDs for all the states and epochs plotted together to show their variations in spectral shape and flux.

PoS(ICRC2023)947

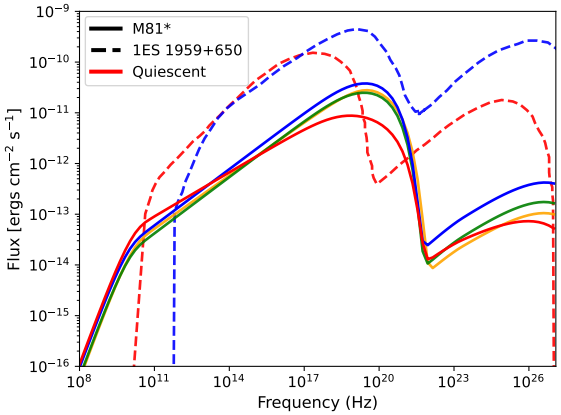

Figure 4: SED of blazar 1ES 1959+650 obtained using a one zone SSC model during quiescent state (red dashed line) and flaring state (blue dashed line) compared with that of M81* during quiescent state (red solid line) and flaring states (blue, green, yellow solid lines).

Parameter	Quiescent State	Flare A	Epoch 2	Epoch 3	Epoch 4	Flare B	Flare C
Spectral index	2.42	2.3	2.3	2.3	2.57	2.26	2.26
Γ_{min}	400	400	400	400	580	400	400
Γ_{max}	1.5×10^{8}	1.5×10^{8}	1.5×10^{8}	1.5×10^{8}	1.5×10^{8}	1.5×10^{8}	1.5×10^{8}
R [cm]	$9.\times10^{16}$	$9.\times10^{16}$	$9.\times10^{16}$	9.0×10^{16}	9.0×10^{16}	9.0×10^{16}	9.0×10^{16}
B [Gauss]	0.004	0.004	0.004	0.004	0.004	0.003	0.003
Doppler factor	4.1	4.1	4.1	4.1	4.1	4.1	4.1
Bulk Γ	3.7	3.7	3.7	3.7	3.7	3.7	3.7
$U'_{e,inj}$[erg cm^{-3}]	1.19×10^{-11}	1.57×10^{-11}	4.20×10^{-11}	7.70×10^{-11}	1.17×10^{-10}	1.21×10^{-11}	1.98×10^{-11}
$P_{e,inj}$[erg s^{-1}]	1.25×10^{35}	1.64×10^{35}	4.39×10^{35}	8.06×10^{35}	1.64×10^{36}	1.27×10^{35}	2.07×10^{35}
U'_B/U'_e	0.017	0.027	0.020	0.017	0.014	0.008	0.007

Table 3: Parameters obtained from the modeling of the SEDs of M81* in different States. Note, the $U'_{e,inj}$ and U'_B are the energy densities in electrons and magnetic field in the jet frame, $P_{e,inj}$ is the jet power in injected electrons. The escape time for each case is taken to be R/c.

[4] Tomar G., Gupta N., 2023, ApJ, 950, 113. doi:10.3847/1538-4357/acd16d

PoS(ICRC2023)947